Numerical research on biomass wastewater treatment using double-partition vessel with off-centered impellers

Wei Zhang[1†], Yijie Yang[1†], Wenmin Qian[2], Longlong Ma[1,3], Lungang Chen[3], Na Liu[1], Ying Liu[1], Yubao Chen[1*]

(1. *School of Energy and Environmental Science, Yunnan Normal University, Kunming 6500500, China*;
2. *Yunnan Research Academy of Eco-environmental Sciences, Kunming 650034, China*;
3. *School of Energy and Environment, Southeast University, Nanjing 210096, China*)

Abstract: Limited by single function, it is difficult for the traditional stirred vessels to meet the requirements of mixing system in biomass wastewater treatment processes. The estimation of biomass wastewater stirring reactor performance by computational fluid dynamics (CFD) during multiphase reactions is important, due to the uncertainty in the numerical results. In this study, a novel double-partition stirred vessel with eccentrically located impellers was developed for the special subject. In addition, many simulations were carried out with the wastewater from biomass ethanol production as the medium to ensure the high reactor performance. The fluid flow was simulated and analyzed using the turbulent RNG k-ε model and multi reference frames. A good agreement is found between the simulation results and the confirmatory experiment. Moreover, the weir crest and interconnected pore were specially designed for the establishment of the circulation of fluid to maintain different technological conditions in the two regions. The distributions of radial velocities and tangential velocities were concentrated near the stirring blade. From the velocity profile, it is deduced that the flow pattern in the stirred vessel is insensitive to Reynolds number. Finally, this simulation study could contribute to the improvement and optimization of the structure, as well as the operation of the novel stirred vessel.

Keywords: biomass, wastewater treatment, double-partition vessel, computational fluid dynamics
DOI: 10.25165/j.ijabe.20231602.7637

Citation: Zhang W, Yang Y J, Qian W M, Ma L L, Chen L G, Liu N, et al. Numerical research on biomass wastewater treatment using double-partition vessel with off-centered impellers. Int J Agric & Biol Eng, 2023; 16(2): 232–240.

1 Introduction

Biomass-based industries such as paper making, sugar production, alcohol fermentation, and food manufacturing produce a large amount of wastewater while obtaining products. The wastewater contains a large amount of cellulose, hemicellulose, starch, sugars, organic acids, and proteins with a high COD value, which seriously pollutes the environment and causes waste of biomass resources. Therefore, the use of suitable processes for efficient treatment is crucial to recover resources, reduce costs, and mitigate the environmental pollution[1].

Mechanically stirred vessels are widely used in the biological wastewater treatment process to perform several operations such as dissolution, crystallization, aerobic fermentation, hydrogenation, chlorination, organic oxidation, and chemical synthesis with suspended catalysts and/or suspension polymerization[2-6]. The treatment of complex multiphase components of biomass wastewater is usually performed using a multi-step method[1,7-9]. Although the traditional single stirred vessels have many advantages such as their simple structure, convenient operation, and mature design, they could not meet the requirements of the complexity and variation of mixed system in biomass wastewater treatment processes[10,11]. However, the series of multiple single stirred reactors increases the investment cost, and the material transportation between reactors reduces the reaction efficiency. Consequently, in this study, a novel double-partition stirred vessel with eccentrically located impellers was developed for the biomass wastewater treatment. This stirred vessel, divided into two regions, can simultaneously perform several stages of the same complex process. The rational design of the stirred vessel ensures a circulation between two zones. In addition, with different technological conditions, the material concentration could be maintained in the two regions by adjusting the circulation rate and rotating speed.

Studies on the performance prediction of stirred vessels have been carried out since the 1980s. In recent years, computational fluid dynamics (CFD) has also become a very powerful tool in the design of stirred vessels, due to the fact that it can provide detailed information on the turbulent flow field in stirred vessels for single-phase and multi-phase applications[12-15]. Furthermore, CFD can perform the visualization analysis of the flow field of the semi-closed and closed pilot reactor[16]. However, the computational results should be validated against experimental data because the calculations depend on several factors, such as the modeling of the geometry, the mesh structure, the boundary conditions, and the used turbulence model. Many CFD modeling studies of turbulent flow in

Received date: 2022-04-25 **Accepted date:** 2022-10-08
Biographies: Wei Zhang, Lecture, research interest: biomass energy and carbon reduction, Email: zw12332111@163.com; **Yijie Yang**, MS candidate, research interest: biomass energy, Email: yy1045858516@163.com; **Wenmin Qian**, Professor, research interest: environmental monitoring, Email: 149685729@qq.com; **Longlong Ma**, Professor, research interest: biomass energy, Email: mall@seu.edu.cn; **Lungang Chen**, Professor, research interest: biomass energy, Email: chenlg@seu.edu.cn; **Na Liu**, Lecture, research interest: carbon reduction, Email: 1261554167@qq.com; **Ying Liu**, Associate Professor, research interest: biomass energy, Email: 542110131@qq.com.
†The authors contributed equally to this work.
***Corresponding author: Yubao Chen**, Professor, research interest: biomass energy, Mailing address: Yunnan Normal University, Kunming 650500, China. Tel: +86-13888821945, Email: chenyubao@ynnu.edu.cn.

agitated vessels have been conducted, especially in stirred reactors for the biomass reaction process[17-23].

In this study, the fluid flow field in double-partition stirred vessel with eccentrically located impellers was developed for complex process of biomass wastewater treatment. The simulations and analysis were performed using the turbulent RNG k-ε model and multi reference frames with the wastewater from biomass ethanol production. The CFD results were compared with experiment results for validation. The flow patterns in the single-phase system were also studied and the velocity components were discussed. Furthermore, the volume of fluid (VOF) scheme is used to simulate the free surface in the multi-phase system. The obtained results provide suggestions for the design of stirred vessels with off-centered agitators, which is important for applications in complex biomass wastewater treatment processes.

2 Materials and methods

2.1 Vessel configuration

The structure and size of the double-partition-eccentrically stirred vessel is shown in Figures 1 and 2, and Table 1. It can be deduced that the vessel has an oblong shape, and it is divided into zones I and II by a clapboard to ensure that several stages of the same complex process can be simultaneously performed in this stirred vessel. The down-pumping and up-pumping impellers are respectively equipped in zones I and II. They are both three-bladed 40° pitched turbines. The baffles were used to eliminate the phenomenon of swirling in the stirred vessel and improve the mixing efficiency. The baffle width was 1/12 of the stirred vessel diameter.

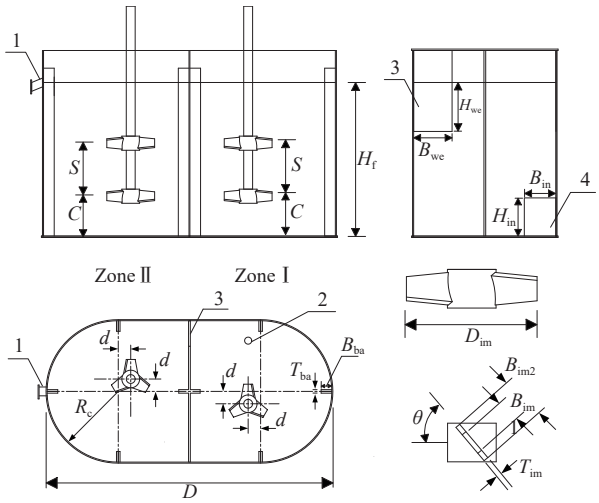

1. Overflow port 2. Feed inlet 3. Weir crest 4. Interconnected pore

Figure 1 Structure of the impeller and vessel

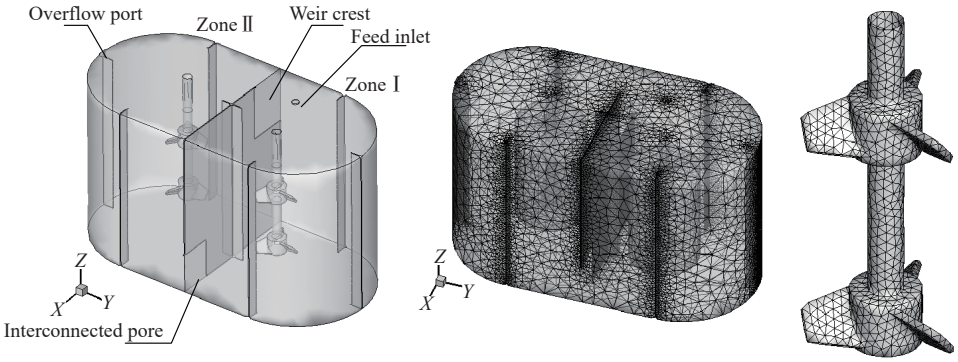

Figure 2 Grid system used in the stirred vessel

Table 1 Geometric specification of the numerical stirred vessel model

Parameters	Values
Distance between impellers S/mm	300
Off bottom clearance C/mm	200
Liquid height H_f/mm/mm	896
Weir crest off free surface H_{we}/mm	304
Weir crest width B_{we}/mm	216
Interconnected pore height H_{in}/mm	216
Interconnected pore width B_{in}/mm	178
Vessel length D/mm	1600
Baffle width B_{ba}/mm	60
Baffle thickness T_{ba}/mm	5
Stirred vessel radius R_c/mm	400
Blade diameter D_{im}/mm	260
Blade width B_{im1}/mm	90
Blade width B_{im2}/mm	50
Blade thickness T_{im}/mm	10
Blade pitch angle θ/(°)	40
Off center d/mm	70

2.2 Model description and computational conditions

The size and structure shown in Figures 1 and 2, and Table 1, were used in the simulation for the comparison with the experimental results. Figure 2 shows the computational grid partitioning. The stirred vessel was divided into three parts; two parts are the inner rotating zones while the third is the outer non-rotating zone. An unstructured tetrahedral grid was densified to deal with large aspect ratios and sharp element angles in the inner rotating zone due to the irregular impeller structure (three-bladed 40° pitched turbines) and the complex reactor structure. Considering the geometrical size difference between the stirred vessel and baffle, a grid was densified to improve the calculation convergence and accuracy. The total number of computational grids was 7×10^5 cells.

2.3 Governing equations

The continuity and momentum equations, based on the conservation principles of mass and momentum in the stirred tank, are given by:

Continuity equation:

$$\frac{\partial \rho}{\partial t}+\nabla\cdot\left(\rho\vec{v}\right)=0 \tag{1}$$

Momentum equation:

$$\frac{\partial}{\partial t}\left(\rho\vec{v}\right)+\nabla\cdot\left(\rho\vec{v}\vec{v}\right)=-\nabla p+\nabla\cdot\left[\mu\left(\nabla\vec{v}+\nabla\vec{v}^{T}\right)-\frac{2}{3}\mu\nabla\cdot\vec{v}I\right]+\rho\vec{g}+\vec{F} \quad (2)$$

where, P is the static pressure, $\rho\vec{g}$ and $\vec{F}$ are respectively the gravitational body force and external body forces (e.g., that arise from interaction with the dispersed phase; $\vec{F}$also contains other model-dependent source terms such as porous-media and user-defined sources), μ is the molecular viscosity, I is the unit tensor, and the second term on the right hand side is the effect of volume dilation. The RNG version of the k-ε model was developed in response to the empirical nature of the standard version of the k-ε model. It has a similar form to that of the standard version of the k-ε model. However, it contains modifications in the dissipation equation to better describe the flows with regions of high strain, such as the flow around a bend or reattachment following the recirculation zone. In addition, a differential equation is solved for the turbulent viscosity[24,25]. This model is used in several studies[26-29]. Therefore, the turbulent RNG k-ε model was used in this study.

The turbulent kinetic energy equation is given by:

$$\frac{\partial}{\partial t}(\rho k)+\frac{\partial}{\partial x_i}(\rho k u_i)=\frac{\partial}{\partial x_j}\left[\alpha_k u_{eff}\frac{\partial k}{\partial x_j}\right]+G_k+\rho\varepsilon \quad (3)$$

The rate of the turbulent kinetic energy equation is expressed as:

$$\frac{\partial}{\partial t}(\rho\varepsilon)+\frac{\partial}{\partial x_i}(\rho\varepsilon u_i)=\frac{\partial}{\partial x_j}\left[\alpha_\varepsilon\mu_{eff}\frac{\partial\varepsilon}{\partial x_j}\right]+C_{1\varepsilon}^{*}\frac{\varepsilon}{k}G_K-C_{2\varepsilon}\rho\frac{\varepsilon^2}{k} \quad (4)$$

where, G_k is the turbulent kinetic energy production term.

$$\mu_{eff}=\mu+\mu_t \quad (5)$$

$$\mu_t=\rho C_\mu\frac{k^2}{\varepsilon} \quad (6)$$

The usual constants of the k-ε turbulent model are listed in Table 2.

Table 2 Constants of the RNG k-ε model

C_μ	$C_{1\varepsilon}$	$C_{2\varepsilon}$	α_ε	α_k
0.0854	1.42	1.68	1.39	1.39

In order to solve the relative rotation between the impeller and baffles, the multiple reference frame method is used as it provides accurate prediction, and demands less computational resources[30-32]. An interface is introduced to exchange all the parameters in the governing equations between the inner and outer zones.

The finite volume method and steady state methods of implicit pressure were used in this study. SIMPEC is used for the Pressure-Velocity Coupling Method, second order upwind discretization scheme for momentum, turbulent kinetic energy, and turbulent dissipation rate. It should be ensured that the iterative convergence is achieved with at least four orders ($1e^{-4}$) of magnitude decrease in the normalized residuals for each solved equation.

Furthermore, the volume of fluid (VOF) scheme is used to simulate the free surface[16,33-36]. In this research, the QUICK discretization scheme was used for Momentum, the First order upwind discretization scheme was used for turbulent kinetic energy and turbulent dissipation rate, the Presto discretization scheme was used for Pressure, and the PISO algorithm was used as Pressure-Velocity Coupling Method. The under-relaxation factors are chosen between 0.2 and 0.5. The small values of the under-relaxation factors are required for the stability of the solution of this interpolation scheme. For transient problems, iterative convergences at each time interval are checked and all the residuals are dropped below four orders ($1e^{-4}$) in almost 10 000 iterations. The time interval is selected as Δt = 0.01 s. Initially, the desired volume fraction of the liquid (water) is uniformly settled at the bottom of the vessel (H_f = 896 mm), while the air is kept stationary in the rest of the tank, as show in Figure 3.

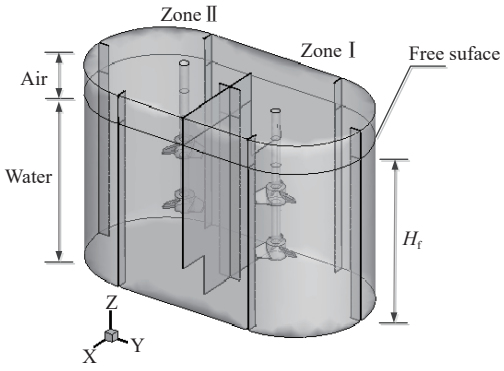

Figure 3 Problem scheme

In the 3D simulations performed in this study, the boundaries depending on the nature of the flow are walls and free-surface. The turbulent flows are significantly affected by the presence of walls. Therefore, how to make the turbulent RNG k-ε model suitable for wall-bounded flows should be taken into consideration. The standard wall functions were used to specify walls, which are based on the proposal of Launder and Spalding, and have been most widely used for industrial flows[36]. In the turbulent RNG k-ε models, the k equation is solved in the whole domain including the wall-adjacent cells. The boundary condition for k imposed at the wall is given by:

$$\frac{\partial k}{\partial n}=0 \quad (7)$$

where, n is the local coordinate normal to the wall.

The production of kinetic energy G_k, and its dissipation rate ε at the wall-adjacent cells, which are the source terms in the k equation, are computed based on the local equilibrium hypothesis. Under this assumption, the production of k and its dissipation rate are assumed to be equal in the wall-adjacent control volume.

Thus, the production of k is computed as:

$$G_k\approx\tau_w\frac{\partial u}{\partial y}=\tau_w\frac{\tau_w}{\kappa\rho C_\mu^{1/4}k_P^{1/2}\Delta y_P} \quad (8)$$

and ε is expressed as:

$$\varepsilon=\frac{C_\mu^{3/4}k_P^{3/2}}{\kappa\Delta y_P} \quad (9)$$

On the walls of the vessel, the impellers and baffles are treated as free-slip and no-slip boundary conditions, respectively. The impellers are rotated with the inner rotating zone.

3 Test verification and analysis

In the simulation calculation and verification experiments, biomass ethanol wastewater was used as the medium. For the validation of the simulation model, the verification experiments were carried out with the same size and structure of the pilot stirred reactor for six cases. The experiment conditions are presented in Table 4. The distribution of 45 monitoring points in the weir is shown in Figure 4. The fluid velocities that were measured in steady-state for case 1, 3, and 5 at midline of weir crest (x = −292 mm) and H = 280 mm, were compared with the simulation results (Figures 5

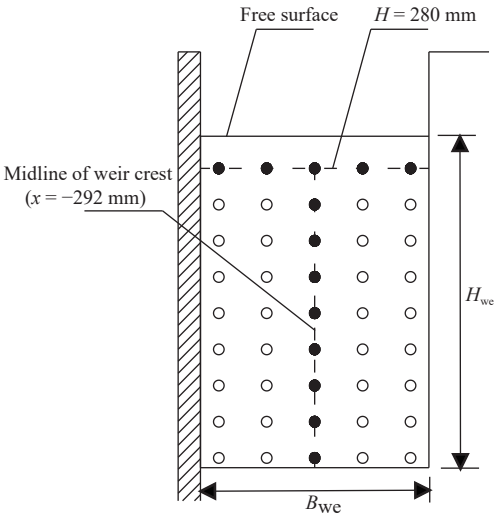

Figure 4 Monitoring point distribution

and 6).

Figure 5 shows comparisons of velocity between the experiment results and simulation results at midline of weir crest (x = −292 mm). It can be observed that the trend of the experimental velocity distribution is consistent with the simulation results. The fluid velocity increased with the height, while it more obviously increased with the Reynolds number. Moreover, the fluid velocity values were fluctuated at locations z/H_{we} = 0.1–0.5, because of the change of part of the fluid velocity direction (from radial velocity to downward axial velocity).

Comparisons of velocity between the experiment results and simulation results at H = 280 mm are shown in Figure 6. The experimental and simulation results are consistent. The experimental flow rate of weir (Q_{weir}), simulation flow rate of weir ($Q_{s\text{-}weir}$), and simulation of flow rate of interconnected pore ($Q_{s\text{-}pore}$) are presented in Table 4. It can be observed that the confirmatory experimental results are consistent with the simulation results. The flow rates of experiments and simulations increased with the Reynolds number, and the maximum relative deviation is 3.08%.

Table 3 Flow rate of the experiment and simulation

case	experiment	simulation	
	Q_{weir} /m³·s⁻¹	$Q_{s\text{-}weir}$ /m³·s⁻¹	$Q_{s\text{-}pore}$ /m³·s⁻¹
1	0.008 95	0.008 92	0.008 93
2	0.007 32	0.007 28	0.007 26
3	0.006 38	0.006 33	0.006 33
4	0.005 70	0.005 62	0.005 61
5	0.003 86	0.003 74	0.003 74
6	0.002 18	0.002 17	0.002 17

4 Results and discussions

4.1 Flow patterns

For the visualization of the flow patterns in the vessel, three intercepting surfaces (side view, z = 150 mm, and z = 750 mm) of velocity vector field, and velocity contour of stirred vessel under case 1, are shown in Figure 7. A presence of downward stream and upward stream is observed near the blade in zone I and zone II (Figure 7b). In addition, near the wall stream, axial movements are observed in upward direction in zone I and downward direction in zone II. Consequently, a typical recirculation loop flow pattern is obtained on the two sides of each impeller, which is created by the jets of the impellers and the radial velocities striking the walls. The shape of the recirculation loops depends on the impeller type.

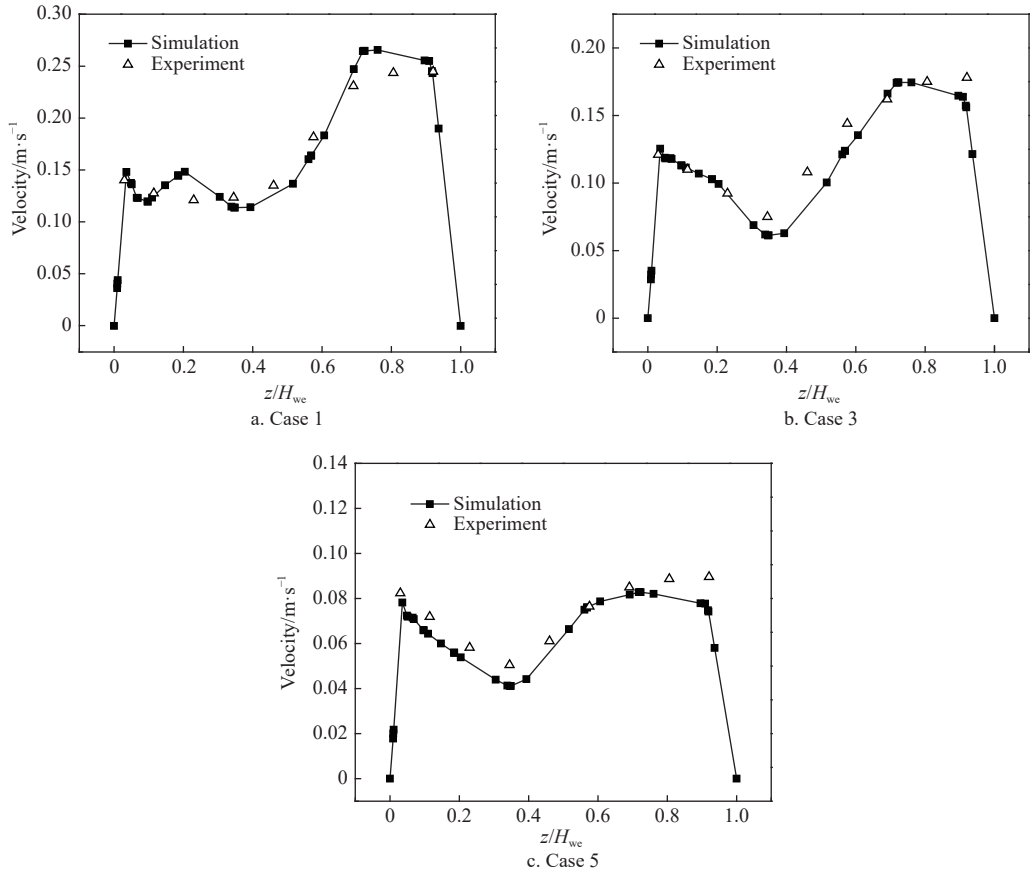

Figure 5 Comparisons of velocity between the experiment results and simulation results at midline of weir crest (x = −292 mm)

Table 4 Experiment conditions

Case	Zone I			Zone II		
	frequency of stirring paddle/Hz	rotating speed of agitator N/r·min^{-1}	$Re\times10^{-4}$	frequency of stirring paddle/Hz	rotating speed of agitator N /r·min^{-1}	$Re\times10^{-4}$
1	69.9	191.0	21.41	59.4	162.2	18.18
2	60.0	159.9	17. 93	50.2	136.3	15.28
3	50.2	138.6	15.54	40.0	108.2	12.13
4	40.0	107.8	12.08	30.2	81.2	9.10
5	30.2	81.6	9.15	20.0	52.5	5.89
6	20.0	53.8	6.03	10.0	24.7	2.77

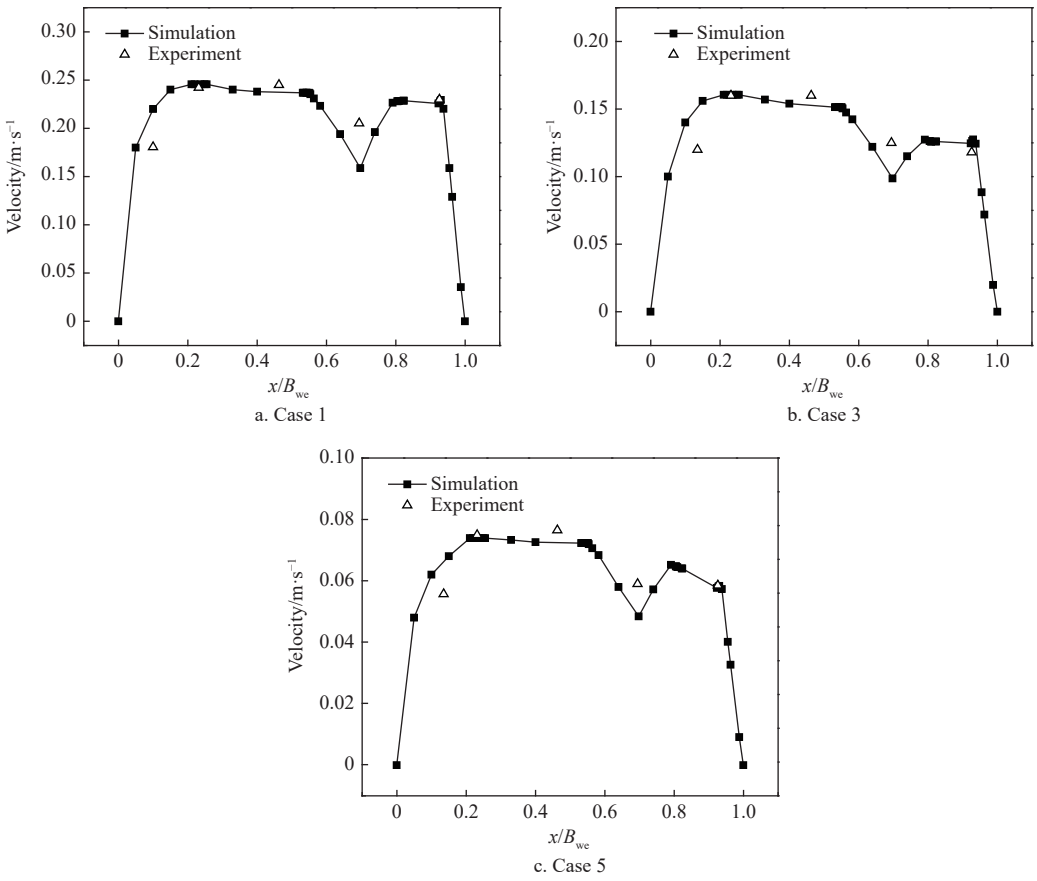

Figure 6 Comparisons of velocity between the experimental results and simulation results at H = 280 mm

Moreover, it is observed that the distribution of radial and tangential velocities in the flow field was concentrated near the blade. Figure 7c shows that one stream in zone I passes through the interconnected pore and enters into zone II, due to the thrust of the down-pumping blade. In zone II, part of the fluid stream through weir crest return to zone I, as shown in Figure 7d. The circulation flow is then formed.

4.2 Free surface

The fluctuation of free surface was obtained by the VOF scheme to determine the change of liquid level with time, to determine the optimal operating conditions of the reactor for treating biomass wastewater. Figure 8 illustrates the simulative distribution of volume fraction of water for case 1, and the change of the free surface with time. The simulation results depend on the time since the VOF scheme is applicable only for the transient problems. The comparisons of unsteady-state and steady-state values of Q_{weir} and Q_{pore} were used to check the stability of the free surface. At t = 20 s, the values of Q_{weir} and Q_{pore} were respectively 0.008 85 m^3/s and 0.008 84 m^3/s, and they were comparable with the values in Table 3, indicating representative free surface pattern. It can be seen from Figure 8 that the height of free surface in zone II is slightly higher than that in zone I, due to the thrust of the down-pumping blade in zone I and the up-pumping blade in zone II. The upward stream was changed to an outward jet stream at free surface in zone II, forming an outward wave. The asymmetric shapes of free surface between zones I and II are then formed.

4.3 Velocity components

Figures 9-11 show the distributions of the velocity component in the stirred vessel at x_1 = 150 mm, y_1 = 330 mm (zone I), x_2 = −150 mm, and y_2 = −330 mm (zone II). The coordinate zero point was in the center of the stirred vessel bottom. The impeller tip speed was calculated as:

$$V_{Tip} = 2\pi N_{rps}\frac{D_{im}}{2} \tag{10}$$

The trends of the distributions of the velocity components, shown in Figures 9-11, can be summarized as follows:

(1) This velocity component shows a maximum value at each turbine (z/H = 0.22, 0.58), which is consistent with the result of the study presented in [37].

(2) The axial velocity was upstream in zone II and downstream

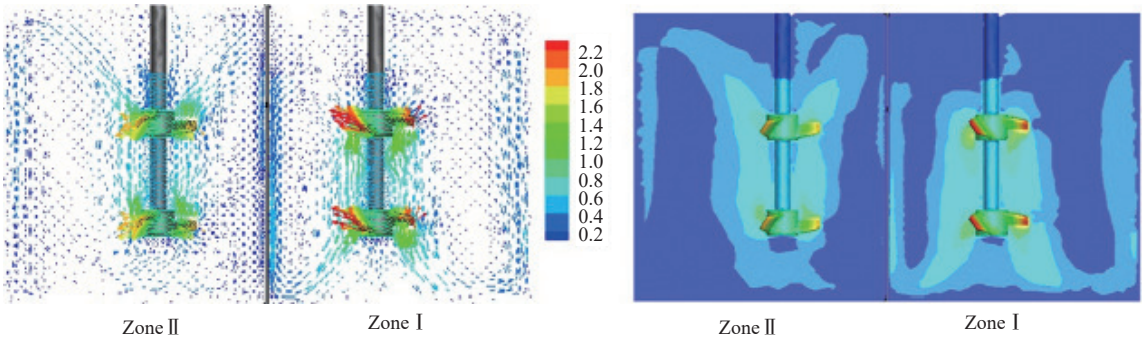

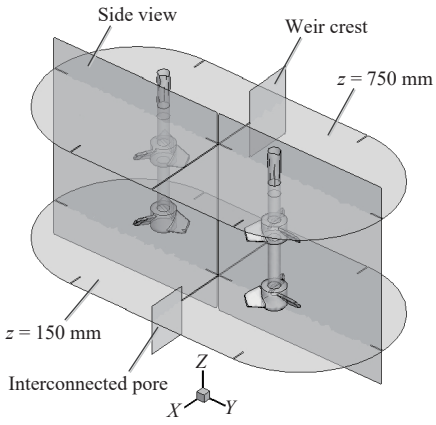

b. Side view

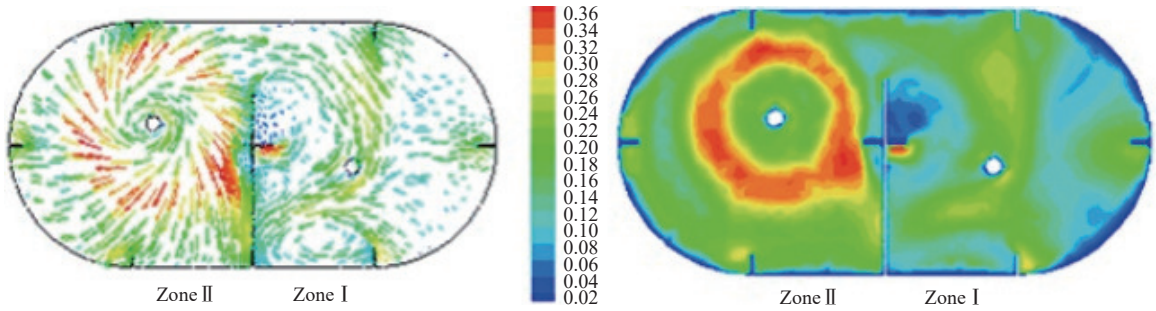

c. z = 150 mm (flow velocity, m·s^{-1})

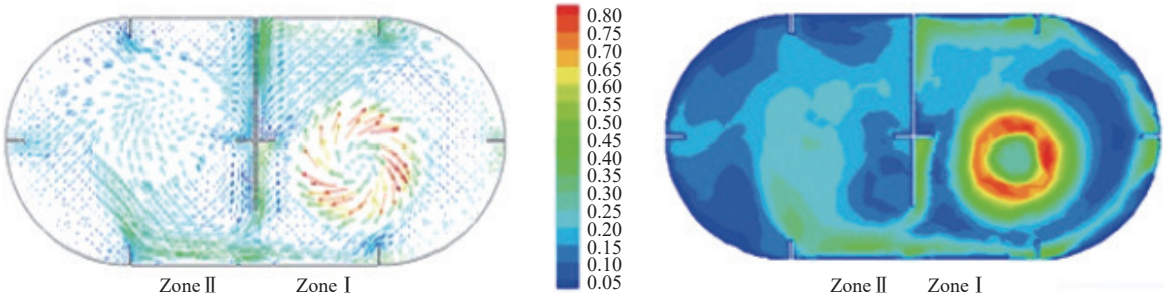

d. z = 750 mm (flow velocity, m·s^{-1})

Figure 7 Velocity vector field and velocity contour of stirred vessel

in zone I, due to the angle of the blades. It can be seen from Figure 9 that the axial velocity was close to zero at z/H = 1 (free surface), which was in accordance with the experimental observation. However, it can be observed from Figures 10 and 11 that the radial velocity and tangential velocity were not zero at z/H = 1 (free surface), because of the change of the fluid velocity direction, from axial velocity to radial velocity and axial velocity.

(3) It can be deduced from Figures 10 and 11 that the distribution of the radial and tangential velocities in the flow field was concentrated near the blade.

(4) The dimensionless velocity profiles ($V_{\text{axial}}/V_{\text{Tip}}$, $V_{tangential}/V_{\text{tip}}$, $V_{\text{radial}}/V_{\text{Tip}}$) coincide basically for six cases in zones I and II. It can be deduced from the velocity profile that the flow pattern in the stirred vessel is insensitive to the Reynolds number.

5 Conclusions

In this study, a novel double-partition-eccentrically stirred vessel was developed, while considering the complexity and

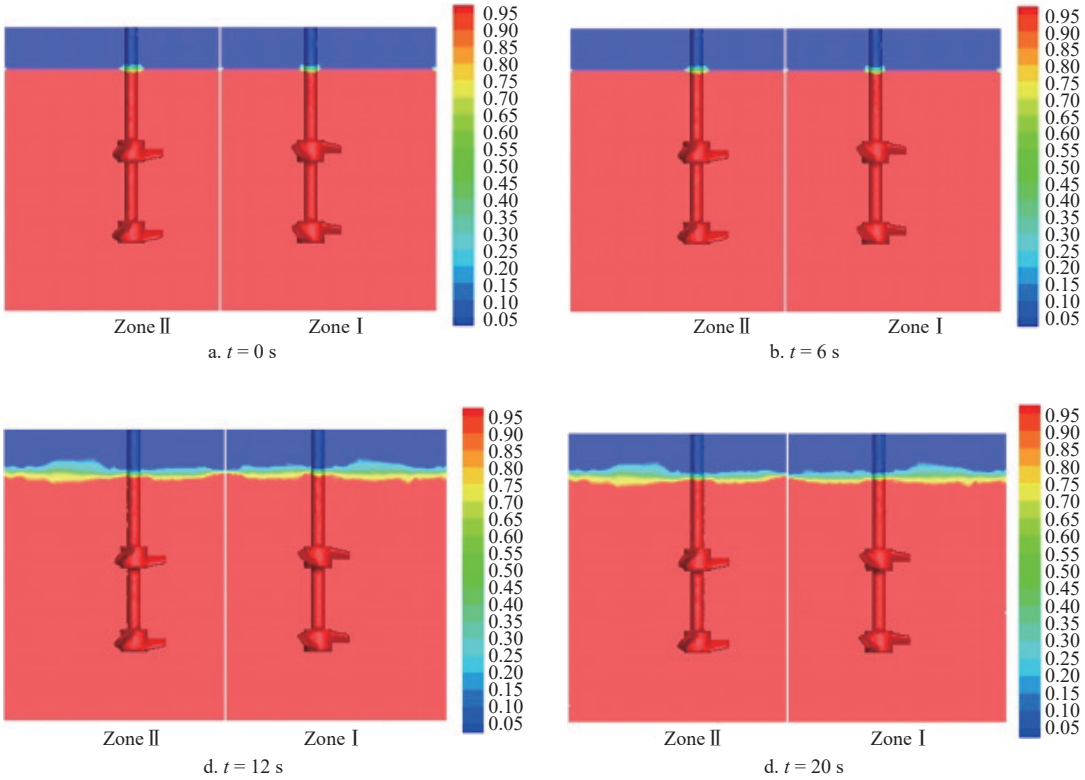

Figure 8 Distribution of volume fraction of water

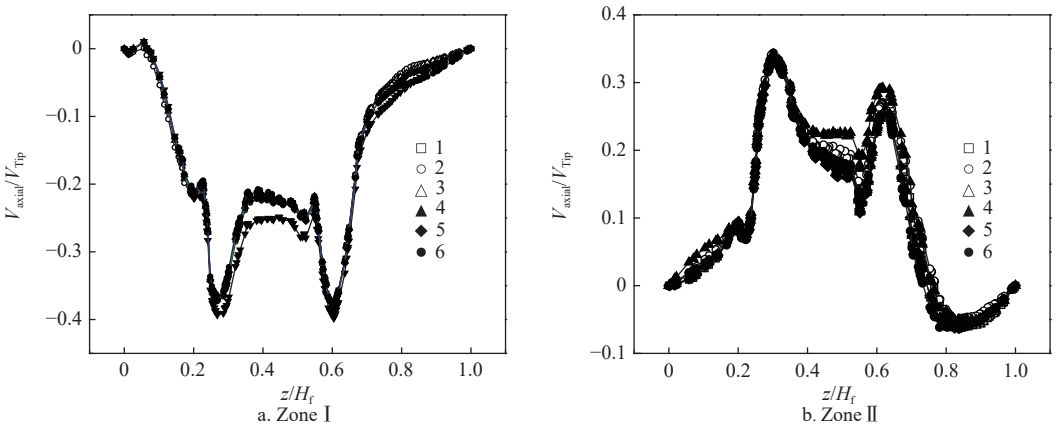

Figure 9 Axial velocity profile

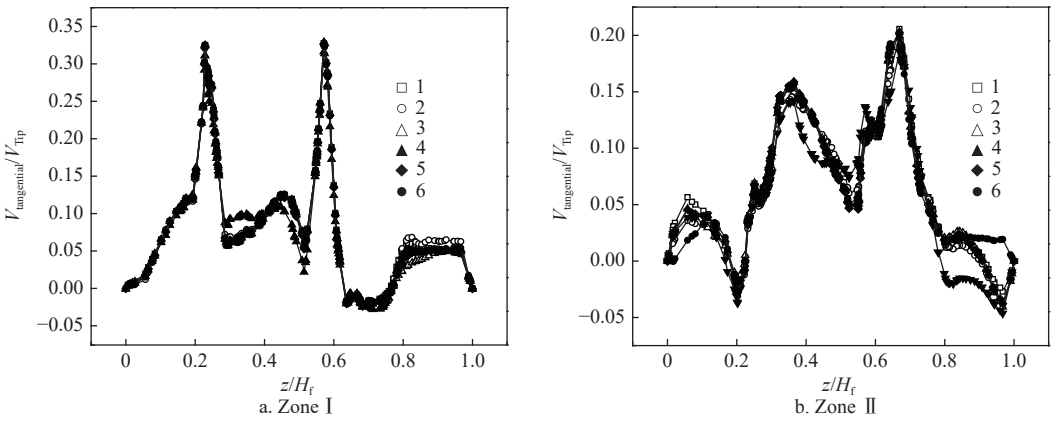

Figure 10 Tangential velocity profile

variation of mixed system in the treatment of complex multiphase components of biomass wastewater. The vessel was divided into two zones to ensure that several stages of the same complex process can be simultaneously performed in this stirred vessel. In addition, two regions are connected by the weir crest and the interconnected pore to ensure the uniform materials contact and improve the reaction efficiency. Using the turbulent RNG *k*-*ε* model and multi reference frames, a CFD based three-dimensional model problem

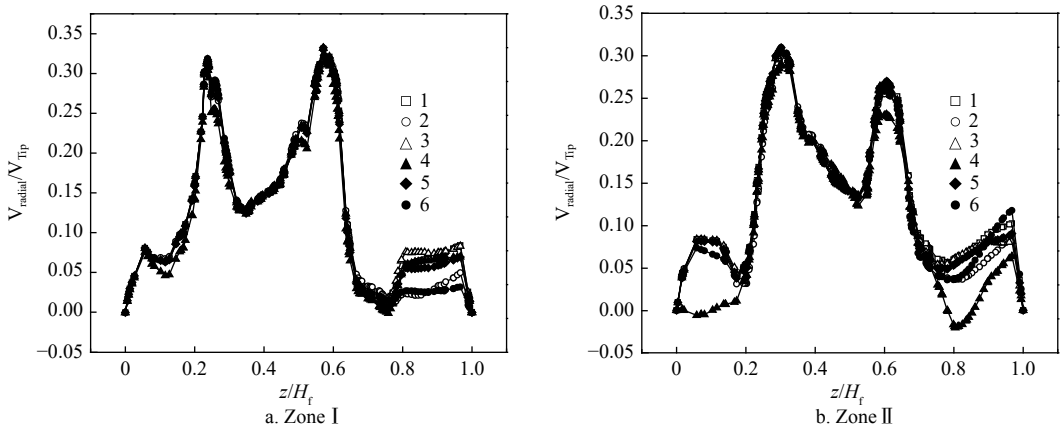

a. Zone Ⅰ b. Zone Ⅱ

Figure 11 Radial velocity profile

was developed to understand the flow pattern and the velocity components characteristics in a stirred vessel driven by three-bladed 40° pitched turbines. Furthermore, using the VOF scheme, the change of the free surface with time was obtained under unsteady-state. Comparisons of the weir flow rate and fluid velocity between the simulation and experimental results were performed. The numerical simulation result was consistent with the experimental result. This indicates that the flow process in the stirred tank can be accurately predicted by the CFD model. It can be deduced from the simulation results of flow pattern and the velocity components that the rational design of weir crest and interconnected pore ensure a circulation between two regions, allowing to establish and maintain different technological conditions in two zones by adjusting the circulation rate and rotating speed. The velocity components curves were consistent for six cases in zones I and II, implying that the flow pattern in the stirred vessel is insensitive to the Reynolds number. This study demonstrates that the CFD model can accurately describe the flow process in double-partition-eccentrically stirred vessel. In addition, it is very useful for the improvement and optimization of the structure and the operation of the novel stirred vessel, as well as the efficient and low-cost treatment of biomass wastewater.

Acknowledgements

This work was supported by the National Natural Science Foundation of China (Grant No. 21868014), Low-carbon Development Guidance Project of Yunnan Province in 2021 (No. 135), Key Sci-Tech Project of China Tobacco Yunnan Industrial Co., Ltd., (Grant No. 2022GY03), Key Project of Yunnan Fundamental Research Program (Grant No. 2019FA004), Yunnan Academician and Expert Workstation (Grant No. 202205 AF150024), Kunming International Sci-Tech Cooperation Base, China (Grant No. GHJD-2020026), Yunnan Sci-Tech Talents and Platform Program (Grant No. 202105AC160058), Scientific research project of Yunnan Environmental Science Society, China (No. XHKYKT006).

Nomenclatures

Symbol	Expression
d /mm	Off left
k /J	Turbulent kinetic energy
k_p /J	Turbulent kinetic energy at point P
n	Local coordinate normal to the wall
Δy_p /mm	Distance from point P to the wall
B_{we} /mm	Weir crest width
B_{in} /mm	Interconnected pore width
B_{ba} /mm	Baffle width
B_{im1}, B_{im2} /mm	Blade width
C /mm	Off bottom clearance
$C\mu$, $C^*1\varepsilon$, $C1\varepsilon$	Model constants
D /mm	Vessel length
D_{im} /mm	Blade diameter
G_k /J	Generation of turbulence kinetic energy
G_b /J	Generation of turbulence kinetic energy due to buoyancy
H_f /mm	Liquid height
H_{we} /mm	Weir crest off free surface
H_{in} /mm	Interconnected pore height
N_{rps} /r·min^{-1}	Stirrer rotation speed
Q'_{weir} /m^3·s^{-1}	Experimental flow of weir
Q_{weir} /m^3·s^{-1}	Simulation flow of weir
Q_{pore} /m^3·s^{-1}	Simulation flow of interconnected pore
R_c /mm	Stirred vessel radius
R_i	Chemical reaction rate
Re	Reynolds number
S /mm	Distance between impellers
T_{ba} /mm	Baffle thickness
T_{im} /mm	Blade thickness
V_{tip} /r·min^{-1}	Impeller tip speed
V_{axial} /r·min^{-1}	Axial velocity
$V_{tangential}$ /r·min^{-1}	Tangential velocity
V_{radial} /r·min^{-1}	Radial velocity
Y_M	Contribution of the fluctuating dilatation in compressible turbulence
ε /%	Turbulent dissipation rate
θ /°	Blade pitch angle
κ	Karman number
μ /N·s·m^{-2}	Molecular dynamic viscosity
ρ /kg·m^{-3}	Density

[References]

[1] Wu J, Cheng S, Cai M H, Wu Y P, Li Y, Wu J C, et al. Applying UV absorbance and fluorescence indices to estimate inactivation of bacteria and formation of bromate during ozonation of water and wastewater effluent. Water Res, 2018; 145: 354–364.

[2] Ali B A, Falleiro L H. Effect of baffle configuration on performance of batch stirred vessel. Korean J Chem Eng, 2022; 38: 1–12.

[3] Lee J. Regime changes of industrial powder mixing in a stirred vessel. Powder Technol, 2021; 392: 306–316.

[4] Giacomelli J J, Van den Akker H E A. A spectral approach of suspending solid particles in a turbulent stirred vessel. AIChE J, 2021; 67: 17097.

[5] Ducoste J J, Clark M M. Turbulence in flocculators: Comparison of measurements and CFD simulations. AIChE J, 1999; 45: 432–436.
[6] Yang K, Wu K, Zhang H. Machine learning prediction of the yield and oxygen content of bio-oil via biomass characteristics and pyrolysis conditions. Energy, 2022; 254: 124320.
[7] Liu X, Deng Q, Zheng Y, Wang D, Ni B-J. Microplastics aging in wastewater treatment plants: Focusing on physicochemical characteristics changes and corresponding environmental risks. Water Res, 2022; 221: 118780.
[8] Li G, Zhang J, Li H, Hu R, Yao X, Liu Y, et al. Towards high-quality biodiesel production from microalgae using original and anaerobically-digested livestock wastewater. Chemosphere, 2021; 273: 128578.
[9] Li G, Lu Z, Zhang J, Li H, Zhou Y, Zayan A M I, et al. Life cycle assessment of biofuel production from microalgae cultivated in anaerobic digested wastewater. Int J Agric Biol Eng, 2020; 13: 241–246.
[10] Wu J, Li Q, Li W, Li Y, Wang G, Li A, et al. Efficient removal of acid dyes using permanent magnetic resin and its preliminary investigation for advanced treatment of dyeing effluents. J Clean Prod, 2020; 251.
[11] Büttner O, Jawitz J W, Birk S, Borchardt D. Why wastewater treatment fails to protect stream ecosystems in Europe. Water Res, 2022; 217: 118382.
[12] Manshoor B, Mdsaufi M F, Zaman I, Khalid A. CFD Analysis of industrial multi-stage impeller in stirred tank with fractal pattern baffled and impeller. Appl Mech Mater, 2015; 773–774: 337–342.
[13] Tamburini A, Brucato A, Ciofalo M, Gagliano G, Micale G, Scargiali F. CFD simulations of early- to fully-turbulent conditions in unbaffled and baffled vessels stirred by a Rushton turbine. Chem Eng Res Des, 2021; 171: 36–47.
[14] Ghasem N. CFD simulation of CO_2 absorption by water-based TiO_2 nanoparticles in a high pressure stirred vessel. Sci Rep, 2021; 11: 1–11.
[15] Russell A W, Kahouadji L, Mirpuri K, Quarmby A, Piccione P M, Matar O K, et al. Mixing viscoplastic fluids in stirred vessels over multiple scales: A combined experimental and CFD approach. Chem Eng Sci, 2019; 208: 115129.
[16] Lin C, Taleghani A D, Kang Y, Xu C. A coupled CFD-DEM numerical simulation of formation and evolution of sealing zones. J Pet Sci Eng, 2022; 208: 109765.
[17] Wang S, Jiang X, Wang R, Wang X, Yang S, Zhao J, et al. Numerical simulation of flow behavior of particles in a liquid-solid stirred vessel with baffles. Adv Powder Technol, 2017; 28: 1611–1624.
[18] Niño-Navarro C, Chairez I, Torres-Bustillos L, Ramírez-Muñoz J, Salgado-Manjarrez E, Garcia-Peña E I. Effects of fluid dynamics on enhanced biohydrogen production in a pilot stirred tank reactor: CFD simulation and experimental studies. Int J Hydrogen Energy, 2016; 41: 14630–14640.
[19] Ri P C, Kim J S, Kim T R, Pang C H, Mun H G, Pak G C, et al. Effect of hydraulic retention time on the hydrogen production in a horizontal and vertical continuous stirred-tank reactor. Int J Hydrogen Energy, 2019; 44: 17742–17749.
[20] Ri P C, Ren N Q, Ding J, Kim J S, Guo W Q. CFD optimization of horizontal continuous stirred-tank (HCSTR) reactor for bio-hydrogen production. Int J Hydrogen Energy, 2017; 42: 9630–9640.
[21] Gakingo G K, Clarke K G, Louw T M. A numerical investigation of the hydrodynamics and mass transfer in a three-phase gas-liquid-liquid stirred tank reactor. Biochem Eng J, 2020; 157: 107522.
[22] Sawant S S, Khadamkar H P, Mathpati C S, Pandit R, Lali A M. Computational and experimental studies of high depth algal raceway pond photo-bioreactor. Renew Energy, 2018; 118: 152–159.
[23] Wu K, Yang K, Wang S, Yu J, Chu C, Luo B, et al. The enrichment of sugars and phenols from fast pyrolysis of bamboo via ethanol-Fenton pretreatment. Bioresour Technol, 2022; 356: 127315.
[24] Zhang H, Wang Y, Sayyar A, Wang T. A CFD-PBM coupled model under entire turbulent spectrum for simulating a bubble column with highly viscous media. AIChE J, 2021. doi: 10.1002/aic.17473
[25] Liu N, Wang W, Wang Y, Wang Z, Han J, Wu C, et al. Comparison of turbulent flow characteristics of liquid-liquid dispersed flow between CFD simulations and direct measurements with particle image velocimetry. Appl Therm Eng, 2017; 125: 1209–1217.
[26] De Lemos M J S, Pedras M H J. Recent mathematical models for turbulent flow in saturated rigid porous media. J Fluids Eng Trans ASME, 2001; 123: 935–940.
[27] Bashiri H, Alizadeh E, Bertrand F, Chaouki J. Investigation of turbulent fluid flows in stirred tanks using a non-intrusive particle tracking technique. Chem Eng Sci, 2016; 140: 233–251.
[28] Jaworski Z, Zakrzewska B. Modelling of the turbulent wall jet generated by a pitched blade turbine impeller. Chemical Engineering Research and Design, 2002; 80(8): 846–854.
[29] Kelly W, Gigas B. Using CFD to predict the behavior of power law fluids near axial-flow impellers operating in the transitional flow regime. Chem Eng Sci, 2003; 58: 2141–2152.
[30] Singh K K, Mahajani S M, Shenoy K T, Patwardhan A W, Ghosh S K. CFD modeling of pilot-scale pump-mixer: Single-phase head and power characteristics. Chem Eng Sci, 2007; 62: 1308–1322.
[31] Ammar M, Chtourou W, Driss Z, Abid M S. Numerical investigation of turbulent flow generated in baffled stirred vessels equipped with three different turbines in one and two-stage system. Energy, 2011; 36: 5081–5093.
[32] Silva P, Tsoutsanis P, Antoniadis A F. Numerical investigation of full helicopter with and without the ground effect. Aerosp Sci Technol, 2022; 122: 107401.
[33] Karim M M, Prasad B, Rahman N. Numerical simulation of free surface water wave for the flow around NACA 0015 hydrofoil using the volume of fluid (VOF) method. Ocean Eng, 2014; 78: 89–94.
[34] Darshan M B, Kumar R, Das A K. Numerical study of interfacial dynamics in flow boiling of R134a inside smooth and structured tubes. Int J Heat Mass Transf, 2022; 188: 122592.
[35] Buhendwa A B, Bezgin D A, Adams N A. Consistent and symmetry preserving data-driven interface reconstruction for the level-set method. J Comput Phys, 2022; 457: 111049.
[36] Xiao J, Wu Q, Chen L, Ke W, Wu C, Yang X, et al. Assessment of different CFD modeling and solving approaches for a supersonic steam ejector simulation. Atmosphere (Basel), 2022; 13.
[37] Sahu A K, Kumar P, Joshi J B. Simulation of flow in stirred vessel with axial flow impeller: zonal modeling and optimization of parameters. Ind Eng Chem Res, 1998; 37: 2116–2130.